Structure and function of the human Gly1619Arg polymorphism of M6P/IGF2R domain 11 implicated in IGF2 dependent growth

Dellel Rezgui, Christopher Williams[1], Sharon A Savage[2], Stuart N Prince, Oliver J Zaccheo, E Yvonne Jones[3], Matthew P Crump[1] and A Bassim Hassan

Cancer Research UK Tumour Growth Control Group, Weatherall Institute of Molecular Medicine, John Radcliffe Hospital, University of Oxford, Headington, Oxford OX3 9DS, UK

[1]Department of Organic and Biological Chemistry, School of Chemistry, University of Bristol, Bristol BS8 1TS, UK

[2]Division of Cancer Epidemiology and Genetics, National Cancer Institute, 6120 Executive Boulevard, EPS/7018, Rockville, Maryland 20852, USA

[3]Cancer Research UK Receptor Structure Research Group, Division of Structural Biology, Wellcome Trust Centre for Human Genetics, University of Oxford, Oxford OX3 7BN, UK

(Correspondence should be addressed to A B Hassan; Email: bass.hassan@imm.ox.ac.uk)

Abstract

The mannose 6-phosphate/IGF 2 receptor (IGF2R) is comprised of 15 extra-cellular domains that bind IGF2 and mannose 6-phosphate ligands. IGF2R transports ligands from the Golgi to the pre-lysosomal compartment and thereafter to and from the cell surface. IGF2R regulates growth, placental development, tumour suppression and signalling. The ligand IGF2 is implicated in the growth phenotype, where IGF2R normally limits bioavailability, such that loss and gain of IGF2R results in increased and reduced growth respectively. The IGF2R exon 34 (5002A > G) polymorphism (rs629849) of the IGF2 specific binding domain has been correlated with impaired childhood growth (A/A homozygotes). We evaluated the function of the Gly1619Arg non-synonymous amino acid modification of domain 11. NMR and X-ray crystallography structures located 1619 remote from the ligand binding region of domain 11. Arg1619 was located close to the fibronectin type II (FnII) domain of domain 13, previously implicated as a modifier of IGF2 ligand binding through indirect interaction with the AB loop of the binding cleft. However, comparison of binding kinetics of IGF2R, Gly1619 and Arg1619 to either IGF2 or mannose 6-phosphate revealed no differences in 'on' and 'off' rates. Quantitative PCR, ^{35}S pulse chase and flow cytometry failed to demonstrate altered gene expression, protein half-life and cell membrane distribution, suggesting the polymorphism had no direct effect on receptor function. Intronic polymorphisms were identified which may be in linkage disequilibrium with rs629849 in certain populations. Other potential IGF2R polymorphisms may account for the correlation with childhood growth, warranting further functional evaluation.

Journal of Molecular Endocrinology (2009) **42,** 341–356

Introduction

The human mannose 6-phosphate/IGF2 receptor (IGF2R) is a large (270 kDa) multi-functional type I membrane protein and *P*-type lectin. The 15 extra-cellular domains of IGF2R bind ligands that are shuttled from the Golgi to the pre-lysosomal compartment and thereafter to and from the cell surface (Ghosh *et al.* 2003). Functional studies in mouse models have shown that IGF2R ligands are involved in embryonic growth, placental development, tumour suppression and signalling.

Mannose 6-phosphate bound to domains 3, 5 and 9 regulates the transport of phosphomannosyl glycoproteins such as lysosomal proteases, and latent transforming growth factor β1 (latent-TGFβ1), where activation of the latter to active TGFβ1 occurs by proteolytic cleavage (Dennis and Rifkin 1991, Hancock *et al.* 2002*a*, *b*, Ghosh *et al.* 2003). IGF 2 (IGF2) binds to domain 11 of mammalian IGF2R with high affinity and specificity ($\sim 10^{-10}$ M), with a fibronectin type II region of domain 13 thought to act as an indirect enhancer of affinity through reduction in 'off rate' (Linnell *et al.* 2001, Williams *et al.* 2007, Brown *et al.* 2008). IGF2 is a small hydrophobic ligand (7·5 kDa) that is normally bound to binding proteins (IGFBP's) that regulate bioavailability through proteolytic cleavage. For example, the potent embryonic growth promoting effect of IGF2 depends on the expression of a developmentally expressed protease, PAPPA2, that cleaves binding proteins to release free IGF2 for signal activation (Conover *et al.* 2004). The binding stochiometry of IGF2 to membrane bound IGF2R is 1:1, and utilises the same binding site on IGF2 that is recognised by binding proteins (Brown *et al.* 2008). IGF2R sequesters free IGF2 ligand and internalises it for intracellular degradation, and so limits activation of the signalling receptors IGF1R and isoform A of the insulin

DOI: 10.1677/JME-08-0154
0952–5041/09/042–341

receptor (Foulstone *et al.* 2005). In the mouse, loss of function of IGF2R results in disproportionate embryonic overgrowth and perinatal lethality that was rescued by the combination with knockout of *Igf2* (Wang *et al.* 1994, Ludwig *et al.* 1996). Moreover, loss of function of IGF2R has been observed in human tumours through loss of heterozygosity and functional missense mutations, with genetic models that also confirm the *Igf2* dependency of tumours (Christofori *et al.* 1994, De Souza *et al.* 1995, Hankins *et al.* 1996, Devi *et al.* 1999, Kong *et al.* 2000, Harper *et al.* 2006). These results suggest that the growth antagonist effects of IGF2R are principally determined by the reduction in free IGF2 ligand supply.

The relative abundance of IGF2 and IGF2R are also regulated at the level of gene expression through genomic imprinting. In all mammals, IGF2 is a maternally silenced (imprinted) gene, with paternal allele expression, whereas IGF2R is normally paternally silenced, with maternal allele expression. Unlike other mammals, IGF2R imprinting in humans is a polymorphic trait, with most individuals having bi-allelic expression that in the mouse results in growth retardation (Kalscheuer *et al.* 1993, Xu *et al.* 1993, Wutz *et al.* 2001). Germ line loss of imprinting of IGF2 has been reported to occur in up to 10% of humans and may be associated with an increased risk of colorectal cancer (Cui *et al.* 2003, Ito *et al.* 2008). Observational data have also correlated blood concentrations of IGF2 and soluble IGF2R with human birth weight and adult height, suggesting that relative supply of ligand and receptor may result in significant growth effects (Ong *et al.* 2000, Garrone *et al.* 2002).

Aside from imprinting, functional dosage of IGF2R may also be modified by polymorphisms that either alters gene expression or protein function. For example, epigenetic mediated reduction in IGF2R expression in cloned sheep accounted for the 'large offspring syndrome' phenotype (Young *et al.* 2001). Single nucleotide polymorphisms have been identified throughout the 140 Kb locus and the 48 exons and introns of human IGF2R (Killian *et al.* 2001). Non-synonymous polymorphisms in coding exons have been mapped to specific domains of the protein. For example, the exon 34 (5002A>G) Gly1619Arg polymorphism generates a non-synonymous modification of domain 11 of IGF2R, and exists in Hardy Weinberg equilibrium in humans (allele frequencies $A=0{\cdot}15$, $G=0{\cdot}85$; Killian *et al.* 2001). Analysis of the Avon Longitudinal Study of Parents and Children prospective cohort of normal mothers and children suggested that babies born with the rarer AA homozygote alleles exhibited slower growth rate kinetics during the first three years of post-natal development, even though circulating IGF2 levels were similar to GG homozygotes and heterozygote controls (Petry *et al.* 2005). A comprehensive analysis of SNPs associated with the later development of cancer has been recently reported with IGF2R haplotypes identified that conferred an increased risk of developing osteosarcoma (Savage *et al.* 2007). In this example, an intron 16 SNP was associated with loss of methylation of a CpG island site that presumably controlled gene expression. The implications of these, and similar SNP association studies, are limited by the lack of functional analysis of associated SNPs, in particular non-synonymous SNPs in ligand binding domains of IGF2R. Here, we report the first comprehensive functional analysis of a non-synonymous IGF2R polymorphism, Gly1619Arg of domain 11, the domain that specifically binds IGF2. We demonstrate that this polymorphism alone has no detectable effects on domain 11 structure, real-time ligand binding kinetics, protein half-life and cell surface distribution. We discuss the implications of these findings with respect to IGF2R function and linkage to other SNPs.

Material and Methods

Plasmids, cloning and reagents

For rat CD4 domains 3 and 4 -IGF2R chimeric constructs (CD4-IGF2R), previously described pEFBOS plasmids containing IGF2R domains 11, 10–13 and 1–15 were utilised (Linnell *et al.* 2001, Zaccheo *et al.* 2006). For membrane-bound IGF2R, full IGF2R insert was derived from ATCC (J03528) using primers (FullIGF2RNheIF2) 5′-atatgctagcGCGATGGGGGCC-GCCGCC-3′ and (FullIGF2RXhoIR2) 5′-gcgcctcgagT-CAGATGTGTAAGAGGTCCTCGTCG-3′, incorporating NheI and XhoI restriction sites respectively. The product was ligated into the pcDNA 3·1(+) vector to generate pcDNA-IGF2R. pEGFP-N1 plasmid was from Clontech (Saint-Germain-en-Laye, France). Protein biotinylation was performed using the BirA biotin-protein ligase from Avidity (CO, USA). Recombinant human IGF2 was from Novozymes GroPep Ltd., (Adelaide, Australia) and latent-TGFβ1 was from R&D systems (Abingdon, UK). L-[^{35}S] methionine and L-[^{35}S] cysteine Redivue Pro-Mix (Radioactive concentration 370 MBq/ml (10 mCi/ml) with respect to L-[^{35}S] methionine at the activity reference date were obtained from Amersham. Methionine/Cysteine-free DMEM and Protein G-Sepharose beads were from Sigma. Mouse anti rat-CD4 antibody (MCA1022R) and mouse anti human-IGF2R (MCA2048) were from AbD Serotec (Oxford, UK), goat anti-mouse PE/Cy5 (M32006) was from Caltag Laboratories (Invitrogen) and rabbit anti-*E*-cadherin was from Santa Cruz Biotechnology Inc., (Heidelberg, Germany). Quick-Change II Site-directed Mutagenesis kit was from

Stratagene (Cheshire, UK) and Phusion Site-directed Mutagenesis kit was from Finnzymes (Espoo, Finland). ImProm-II reverse transcription system was from Promega. Surface plasmon resonance (SPR) buffers, chips and consumables were from GE Healthcare (BIAcore, Chalfont, UK). The FACSCalibur system used for flow cytometry was from Becton Dickinson (Oxford, UK).

Site-directed mutagenesis

In the pEFBOS plasmids, Gly1619Arg mutant constructs were generated using the Quick-Change II kit according to the manufacturer's protocols, using primers (G1619R F) 5′-CGTGTGCAGGCCTGAGGC-C*A*GGCCAACCAATAGGCC-3′ and (G1619R R) 5′-GGCCTATTGGTTGGCC*T*GGCCTCAGGCCTGCAC-ACG-3′. For IGF2R domains 11, 10–13 and 1–15 these are termed CD4-11, CD4-10–13 and CD4-1–15. In the pcDNA-IGF2R plasmid, Gly1619Arg mutant constructs were generated using the Phusion kit according to the manufacturer's protocols, using primers (G1619R-phus-F) 5′-GCC*A*GGCCAACCAATAGGCC-CATGCTCATCT-3′ and (G1619R-phus-R) 5′-CTC-AGGCCTGCACACGAAACTGATCACACTC-3′. The mutations were confirmed by DNA bi-directional sequencing performed by the sequencing service (School of Life Sciences, University of Dundee, Scotland) using Applied Biosystems Big-Dye Version 3.1 chemistry on an Applied Biosystems model 3730 automated capillary DNA sequencer.

IGF2R domain 11 G1619R

To construct IGF2R domain 11 Gly1619Arg expression vector, domain 11 Gly1619Arg was amplified by PCR from pEFBOS-IGF2R-domain11 Gly1619Arg and cloned into the *Nde*I and *Xho*I restriction sites of pET26b (Novagen) using standard methods. The authenticity of the clones was verified by sequencing. Wild-type domain 11 had been previously cloned into pET22b for *Escherichia coli* expression (Brown *et al.* 2002). ^{15}N-labelled wild-type and Gly1619Arg domain 11 were expressed in *E. coli* BL21(DE3) grown in M9 media supplemented with 1 g/l of $^{15}NH_4Cl$ as the sole nitrogen source and refolded using established protocols (Williams *et al.* 2007). Owing to slightly different cloning strategies, wild-type domain 11 had a C-terminal hexahistidine tag while the Gly1619Arg domain 11 construct lacked any additional amino acids.

NMR spectroscopy

NMR samples typically contained ~ 250 μM protein dissolved in 600 μl of 20 mM sodium acetate (pH5.5), 1 mM EDTA, 1 mM benzamidine and 100 μM NaN_3 in 95% H_2O/5% D_2O. Two dimensional ^{1}H-^{15}N heteronuclear single quantum coherence spectra were recorded at 25 °C on a Varian 600 MHz INOVA spectrometer equipped with a triple resonance probe. Spectra were acquired with 1024 ^{1}H complex points in the t2 dimension and 128 points in the ^{15}N dimension, and spectral widths of 7000 Hz in ^{1}H and 2000 Hz in ^{15}N. Data were processed using NMRPipe (Delaglio *et al.* 1995) and analysed with CCPN Analysis version 1.015 (Vranken *et al.* 2005).

Expression of CD4-IGF2R chimeras and membrane bound IGF2R

The CD4-IGF2R chimeric constructs were transiently expressed in 293T cells using Fugene 6.0 (Roche). Briefly, 4 μg DNA and in a 6:1 plasmid:Fugene ratio were added to cells and grown for 5 days in serum free media (DMEM; Sigma-D5796) with 4500 mg/l glucose, L-glutamine (584 mg/l), $NaHCO_3$ (3·7 g/l) and pyrodoxyl HCl (4 mg/l) with added 50 u/ml penicillin, 50 μg/ml streptomycin. Spent culture supernatants were collected, and cells were cleared by centrifugation. Cell lysis and recombinant CD4-IGF2R chimeras' detection was with a CD4 sandwich ELISA as described (Davis *et al.* 1990). Protein biotinylation, SDS PAGE and western blotting were also performed as previously described (Linnell *et al.* 2001, Zaccheo *et al.* 2006). The full length IGF2R constructs were transiently co-expressed in 293T cells with eGFP plasmid using lipofectamine (10 μl) (Invitrogen) using 3·6 μg pcDNA-IGF2R and 0·4 μg eGFP-N1 plasmid in antibiotic-free growth media (DMEM with 2mM glutamine and 10% fetal bovine serum). The medium was changed 24 h post-transfection to serum-free medium, and cells were prepared for flow cytometry 48 h post-transfection.

Surface plasmon resonance kinetic analysis

Kinetic analysis by SPR was conducted as previously described (Zaccheo *et al.* 2006) using a BIAcore 3000 biosensor (BIAcore). All SPR experiments were performed at 25 °C in HBS-EP (10 mM Hepes (pH 7.4), 150 mM NaCl, 3 mM EDTA and 0·005% (v/v) surfactant P20) at a flow-rate of 40 μl/min. After pre-conditioning, the sensor chip with three 1 min injections of 1 M NaCl, 50 mM NaOH, either ~ 600 RU of recombinant biotinylated CD4-11, ~ 1600 RU of recombinant biotinylated CD4-10–13 or ~ 3300 RU of recombinant biotinylated CD4-1–15 were immobilised on a Sensor Chip SA by affinity capture to streptavidin. Kinetic experiments consisted of a 2–5 min injection of analyte followed by a 150–200 s dissociation phase in HBS-EP running buffer, after which the binding surface

was regenerated with a 2 min injection of 2 M $MgCl_2$. Kinetic parameters were determined by global fitting of sensorgrams to a two-state (conformational change) binding model using BIA evaluation software version 4.0.1. In all cases, the minor component made an insignificant contribution to the overall affinity and, as such, only the kinetic parameters of the major binding component were used. For each interaction, the dissociation affinity constant (K_D) were also calculated by fitting of the response of each concentration at equilibrium to a steady-state affinity model using BIAevaluation.

Using the SA sensor chip with immobilised WT CD4-1–15 and G1619R CD4-1–15, competition assay experiments were run at a flow-rate of 40 µl/min and consisted of a co-inject of a first 100 µl injection of either (130 nM) recombinant human IGF2 or (30 nM) latent TGFβ1, followed by a second 100 µl injection of a 1:1 mixture of both analytes at the same above concentrations or 1:1 mixture of one analyte with buffer. A control experiment was run on the same sensor chip, where a co-inject of a first 100 µl injection of buffer (HBS-EP), followed by a second 100 µl injection of a 1:1 mixture of each analyte at the same above concentrations with buffer.

Analysis of the competition experiments were performed by quantifying the amounts of bound analyte from the second injection of each co-inject. This was assessed from the response amplitude (RU) and compared with control injections. For both kinetic and competition analyses, a blank flow-cell was used for in-line reference subtraction of changes due to differences in refractive index of running buffer versus sample and a buffer-only injection was used to subtract instrument noise and drift. Injections were performed in duplicate for each concentration and in a randomised order.

Quantitative RT PCR

RNA was extracted from 293T cells 5 days post-transfection, using Trizol (Invitrogen) in accordance with the manufacturer's protocol. The extracted RNA was then treated with DNase (Amplification grade, Invitrogen) and reverse transcribed. Subsequently, real-time PCR was performed using the SYBR Green QuantiTect RT-PCR Kit (Qiagen) and the Mx3000P real-time cycler in accordance with the manufacturer's instructions. Data were analysed in accordance with manufacturers' instructions.

[^{35}S]-methionine and [^{35}S]-cysteine pulse-chase

In 9·5 cm^2 6-well plates, 293T cells were transfected by Fugene 6 using 1 µg plasmid DNA and a 6:1 plasmid:Fugene ratio in growth media (DMEM with 2 mM glutamine, antibiotics and 10% fetal bovine serum). Transfected cells were incubated at 37 °C in a humidified incubator supplied with 5% CO_2 for 24 h

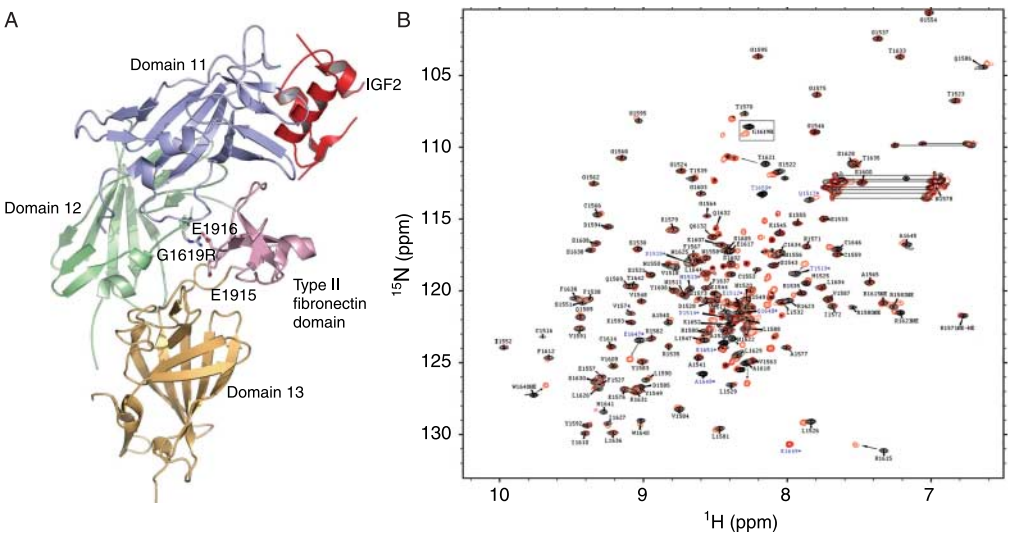

Figure 1 Structural localisation of Gly1619 of IGF2R domain 11. (A) Crystal structure of IGF2R domain 11–13 bound to IGF2(2) (PDB: 2V5P). Gly1619 is located in a long loop between β-strands G and H. Modelling of the arginine replacement of glycine (Gly1619Arg) suggests that the Gly1619Arg polymorphism may interact with a group of charged residues of the fibronectin type II (FnII) domain of domain 13, rendered as pink sticks, e.g. Glu1916 and Glu1915. (B) Comparison of the ^{1}H-^{15}N HSQC spectra of wild-type (Gly1619, black) and Arg1619 (red) domain 11 recorded at 600 MHz at pH5.5, 25 °C. Side chain NH_2 groups of Asn and Gln are indicated by lines parallel to the ^{1}H axis and the Gly1619Arg polymorphism is boxed. Changes in the spectra due to differences in the constructs are highlighted with an asterisk.

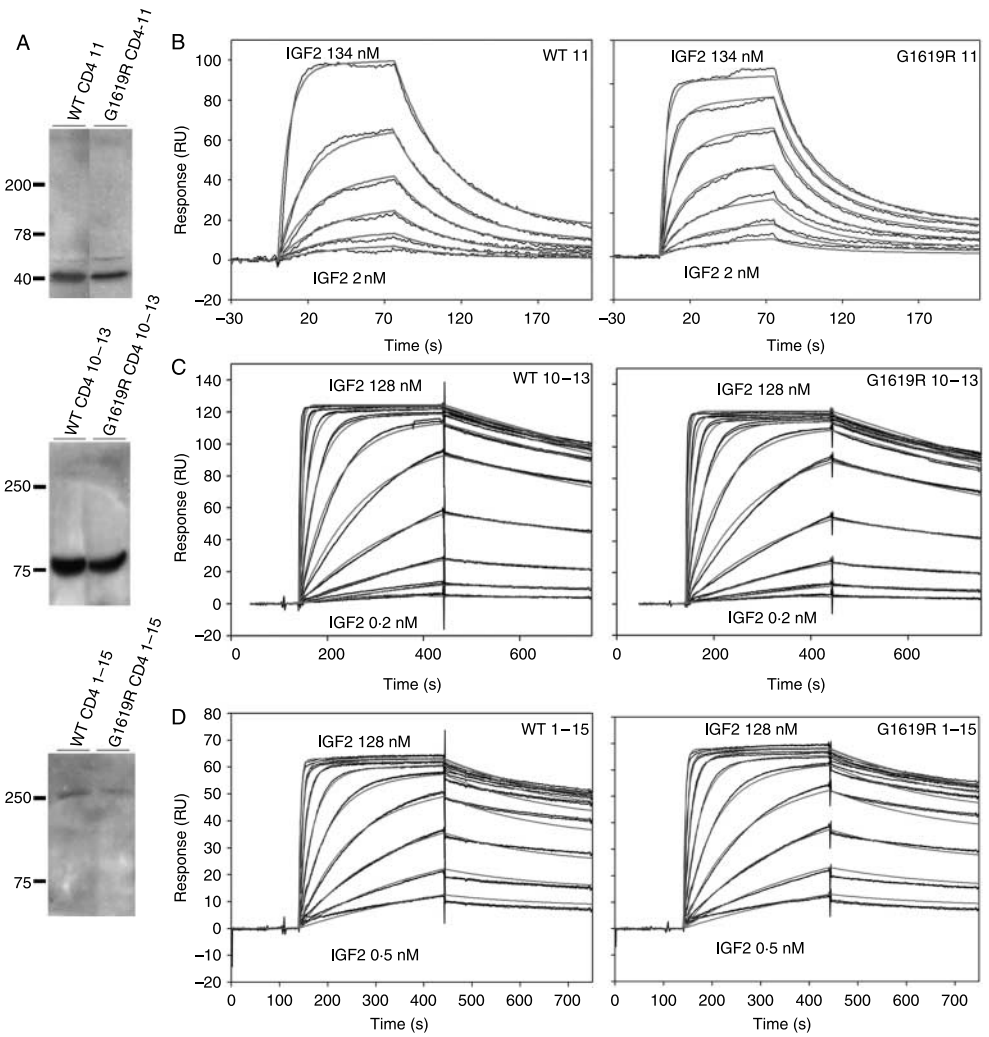

Figure 2 Protein expression and real-time kinetic analysis of wild-type and Gly1619Arg IGF2R binding to IGF2. (A) Western blot detection of the expressed and biotinylated recombinant proteins. Soluble CD4 chimeric proteins were biotinylated, subjected to SDS-PAGE and directly probed with streptavidin conjugated to alkaline phosphatase. (B) Representative sensorgrams depicting injections of recombinant IGF2 at 2, 4, 8, 16, 33 and 134 nM binding to immobilised CD4-11 chimeric proteins; WT domain 11 (WT 11) and Gly1619Arg (abbreviated to G1619R) domain 11 (G1619R 11). (C) and (D) Representative sensorgrams depicting duplicate injections of recombinant IGF2 at 0·2, 0·5, 1, 2, 4, 8, 16, 32, 64, 128 nM binding to CD4-11 chimeric proteins; wild-type recombinant 10–13 domains (WT 10–13), Gly1619Arg recombinant 10–13 domains (Gly1619Arg 10–13), wild-type recombinant 1–15 domains (WT 1–15) and Gly1619Arg recombinant 1–15 domains (G1619R 1–15). Constructs and ranges of analyte concentrations are indicated. Grey lines represent the global fitting of the data set to a two-state (conformational change) binding model (see also Table 1).

prior to initiation of pulse-chase. Cells were first washed twice with PBS and incubated for 30–60 min in 1 ml starvation medium (methionine/cysteine-free DMEM, 50 u/ml penicillin, 50 µg/ml streptomycin and 2 mM glutamine). For metabolic labelling, the starvation medium was replaced with 500 µl/well of pulse medium (starvation medium +0·1 mCi/ml [^{35}S]-methionine and [^{35}S]-cysteine Redivue Pro-Mix) and pulsed for 1 h or 12 h at 37 °C and 5% CO_2. Metabolic labelling was stopped by adding 500 µl per well of chase medium (starvation medium supplemented with cold 5 mM cysteine and 5 mM methionine), washed and incubated 1 ml per well of chase medium. After the selected chase time, supernatants were recovered, centrifuged at 5000***g*** for 5 min, immediately snap-frozen in liquid nitrogen and stored at −80 °C until all chase samples were collected. For each selected chase time, cells were incubated for 30 min on ice (4 °C) in 500 µl/well lysis

Table 1 BIAcore kinetic analysis of IGF2 and latent TGFβ1 binding to recombinant IGF2R chimeric domains

	Immobilised ligand on SA sensor chip	k_{a1} (1/Ms) ($\times 10^5$)	k_{d1} (1/s) ($\times 10^{-2}$)	k_{a2} (1/Ms) ($\times 10^{-3}$)	k_{d2} (1/s) ($\times 10^{-3}$)	K_D (M) ($\times 10^{-9}$)	Relative K_D	X^2	Steady state K_D (M) ($\times 10^{-9}$)
Analyte									
IGF2	CD4 IGF2R-Dom11								
	WT	8·65	2·68	2·01	1·37	31·2	1	2·1	36·5
	Gly^{1619}Arg	7·03	2·44	1·27	2·05	34·7	1·11	3·2	36·3
	CD4 IGF2R-Dom10-13								
	WT	1·23±0·14	1·72±0·5	3·51±2·19	2·15±0·82	1·35±0·27	1	11·1	2·76±0·31
	Gly^{1619}Arg	1·21±0·12	1·68±0·43	3·85±2·82	4·14±1·36	1·37±0·26	1·01	11·2	2·83±0·31
	CD4 IGF2R-Dom1-15								
	WT	1·75±0·19	2·15±0·13	2·29±0·22	4·68±1·79	1·27±0·2	1	1·6	1·99±0·3
	Gly^{1619}Arg	1·67±0·16	2·09±0·11	2·54±0·23	1·86±0·6	1·29±0·2	1·01	0·9	2·09±0·3
Latent TGFβ1	CD4 IGF2R-Dom1-15								
	WT	3·33	0·61	1·93	0·0016	18·3	1	2·4	/
	Gly^{1619}Arg	2·99	0·58	1·9	0·0033	19·4	1·06	2·5	/

buffer (50 mM Tris–HCL pH 7.4, 150 mM NaCl, 2 mM $MgCl_2$, 1:1000 protease inhibitor cocktail (Sigma P3840), 1:1000 PMSF from a 200 mM Stock in Isopropanol). Cell lysates were then snap frozen in liquid nitrogen and stored at −80 °C. For immunoprecipitation (IP), liquid scintillation counting and protein assays, unfrozen samples were centrifuged at 10 600***g*** for 10 min to pellet the nuclei and remove debris. Immuno-precipitation was performed using 20 µl Protein G-Sepharose (2 mg/ml) beads for each sample, where PBS-washed beads and 1 µl antibody were incubated with slow rotation overnight at 4 °C with either 250 µl of the recovered supernatants or 50 µl cell lysates in a total volume 600 µl. Pellets were then washed three times with PBS and prepared for SDS-PAGE analysis by final re-suspension in 15 µl/pellet of 5×Sample buffer (200 mM Tris–HCl pH 6.8, 10% SDS, 50% glycerol, 5% 2-mercaptoethanol, 0·05% bromophenol blue) and 5 min boiling at 95 °C. Immuno-precipitation products were loaded in 5% (w/v) polyacrylamide gels and were run at 200 V for 35 min, dried on 0·5 mm Whatman filter paper in a vacuum-heated gel dryer and exposed to a BioRad phosphor imaging screen.

Scanning densitometry was used to quantify radioactivity, and values were expressed relative to a loading control of total radioactivity in each sample. The latter was determined by total liquid scintillation counting using PerkinElmer scintillation cocktail (Ultima Gold LLT).

Flow cytometry

Cells were detached from plates using 0·1 mM EDTA. For cell surface detection with an intact cell membrane, cells were not fixed or permeablised, however, for total expression, cells were fixed in 1ml paraformaldehyde (2% w/v in PBS, pH 7.4) at 4 °C for 30 min and permeablised in 0.1% v/v Triton in 2% w/v paraformaldehyde at 4 °C for 30 min.

Cells were treated with 1 ml buffer (1% BSA in PBS) and stained using 100 µl buffer with 1:50 diluted primary antibody (AbD Serotec mouse anti-human IGF2R CD222) and incubated at room temperature for 1 h at 4 °C. Cells were than washed and incubated in 100 µl buffer with 1:50 diluted secondary antibody (Caltag goat anti-mouse PE/Cy5) for 1 h at 4 °C. Cells were analysed using a Becton Dickinson FACSCalibur system and data were analysed using WinMDI 2.8 software.

Single nucleotide polymorphism bioinformatics analyses

The allele frequency of rs629849 and linkage disequilibrium of *IGF2R* around this SNP was investigated using publicly available genotype data from the HapMap (Han Chinese, Japanese, and Yoruba) (Frazer *et al.* 2007), SNP500Cancer (African/African American, Caucasian, Hispanic, and Pacific Rim) (Packer *et al.* 2006) and the Multi-Ethnic Cohort (Black, Hawaiian, Japanese, Latino, and White) (Kolonel *et al.* 2004). Haploview (version 4.1) was used to calculate measures of linkage disequilibrium (LD). These measures included absolute D′ (a measure of the covariance of allele counts for two SNPs under the assumption of Hardy–Weinberg equilibrium), the 95% confidence intervals for D′, LOD scores (log of the likelihood ratio, a measure of the confidence in the value of D′), and the

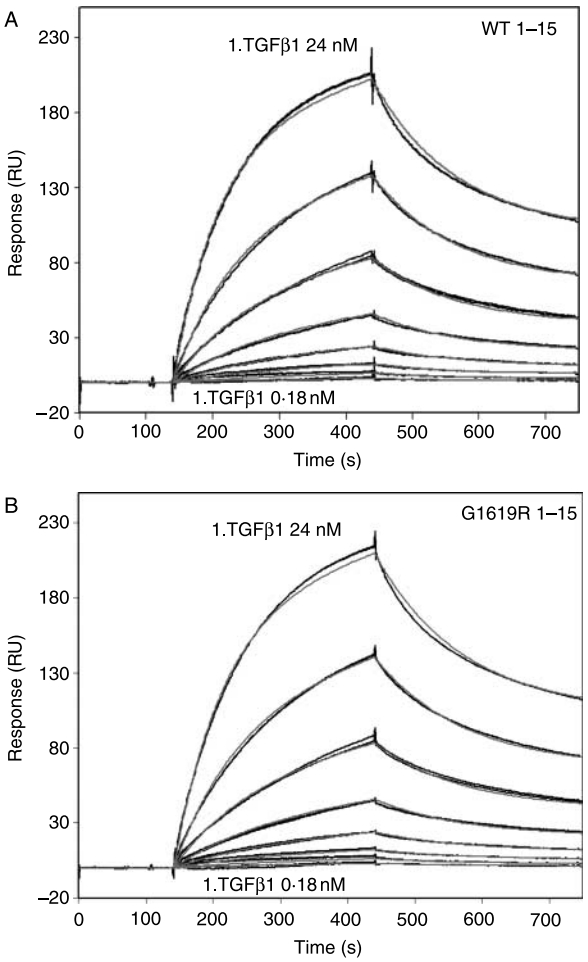

Figure 3 Real-time kinetic evaluation of the binding of latent-TGFβ1 to wild-type and G1619R IGF2R domains 1–15. Representative sensorgrams depicting duplicate injections of recombinant latent TGFβ1 at 0·18, 0·37, 0·75, 1·5, 3, 6, 12 and 24 nM binding to immobilised CD4-11 chimeric proteins; wild-type recombinant 1–15 domains (WT 1–15) (A) and Gly1619Arg recombinant 1–15 domains (G1619R 1–15) (B). Constructs and ranges of analyte concentrations are indicated. Grey lines represent the global fitting of the data using a two-state (conformational change) binding model (see also Table 1).

R-squared (R^2) statistic (correlation coefficient for the pairwise comparison of the SNPs) (Barrett *et al.* 2005).

Results

Structural location, conformation and modelling of Gly1619Arg

We first determined the localisation of Gly1619 in relation to the IGF2 binding site of human IGF2R domain 11. We utilised our high resolution NMR and X-ray crystallographic structures of human IGF2 bound to 11–13 of IGF2R at 4·1 Å (Williams *et al.* 2007, Brown *et al.* 2008). Both the solution structure of domain 11 of IGF2R, and the modelled IGF2 binding interaction using HADDOCK, located Gly1619 in the GH loop region, distant from the cluster of differentiation, AB and FG that formed the IGF2 binding site (Fig. 1A) (Williams *et al.* 2007, Brown *et al.* 2008). IGF2 induced conformational changes in domain 11 structure detected by NMR were predominantly located in the binding loops (AB, cluster of differentiation and FG loops) rather than the carbon backbone of the β-barrel structure.

Detailed examination of domain 11 ^{1}H-^{15}N heteronuclear single quantum coherence (HSQC) spectra showed that Arg1619 modification did not significantly alter protein conformation when compared with Gly1619 (Fig. 1B). Moreover, comparison of the crystal structures of ligand free domains of 11–14 at 2·9 Å, and domains 11–13 with IGF2 bound at 4·1 Å, also showed no conformational change in either the localisation or juxtaposition of G1619 (see Supplementary Figure S3 of Brown *et al.* (2008)). Modelling of the arginine replacement of glycine revealed a number of new potential electrostatic interactions with Glu1916 and Glu1915 of the fibronectin type II (FnII) domain of domain 13 (Fig. 1A). These new interactions may help to stabilise the fibronectin type II domain, and alter the orientation of the interaction with the AB loop of domain 11 that can modify IGF2 binding (Brown *et al.* 2008). The FnII residues interacting with the AB loop are on the same long loop as those that could possibly interact with Gly/Arg1619, namely Ser1921 and Arg1922, and possibly Trp1639. As a result of the location of Gly1619 between domain 11 and 12, it is also possible that Arg1619 may alter the conformation between domains on ligand binding of IGF2, which may not only alter IGF2 interactions with domain 11, but may also alter the subsequent binding of mannose 6-phosphate to domain 3, 5 and 9.

Real-time analysis of IGF2 ligand binding using SPR

Analysis of the domain 11 structure suggested that the Gly1619Arg polymorphism may alter the IGF2 binding interaction indirectly by modifying the interaction between the AB loop of IGF2R domain 11 and the FnII domain of domain 13. We had previously mutated the AB loop residues and identified Glu1544 as an important residue in the interaction with IGF2, and when mutated to a Lys a sixfold enhanced affinity to IGF2 was observed (Zaccheo *et al.* 2006). Moreover, when we deleted the FnII domain in domain 13, we detected an increased 'off rate' of the interaction by tenfold with IGF2, which could be partially rescued by the Glu1544Lys mutation (Brown *et al.* 2008). By utilising protein expression systems we have previously

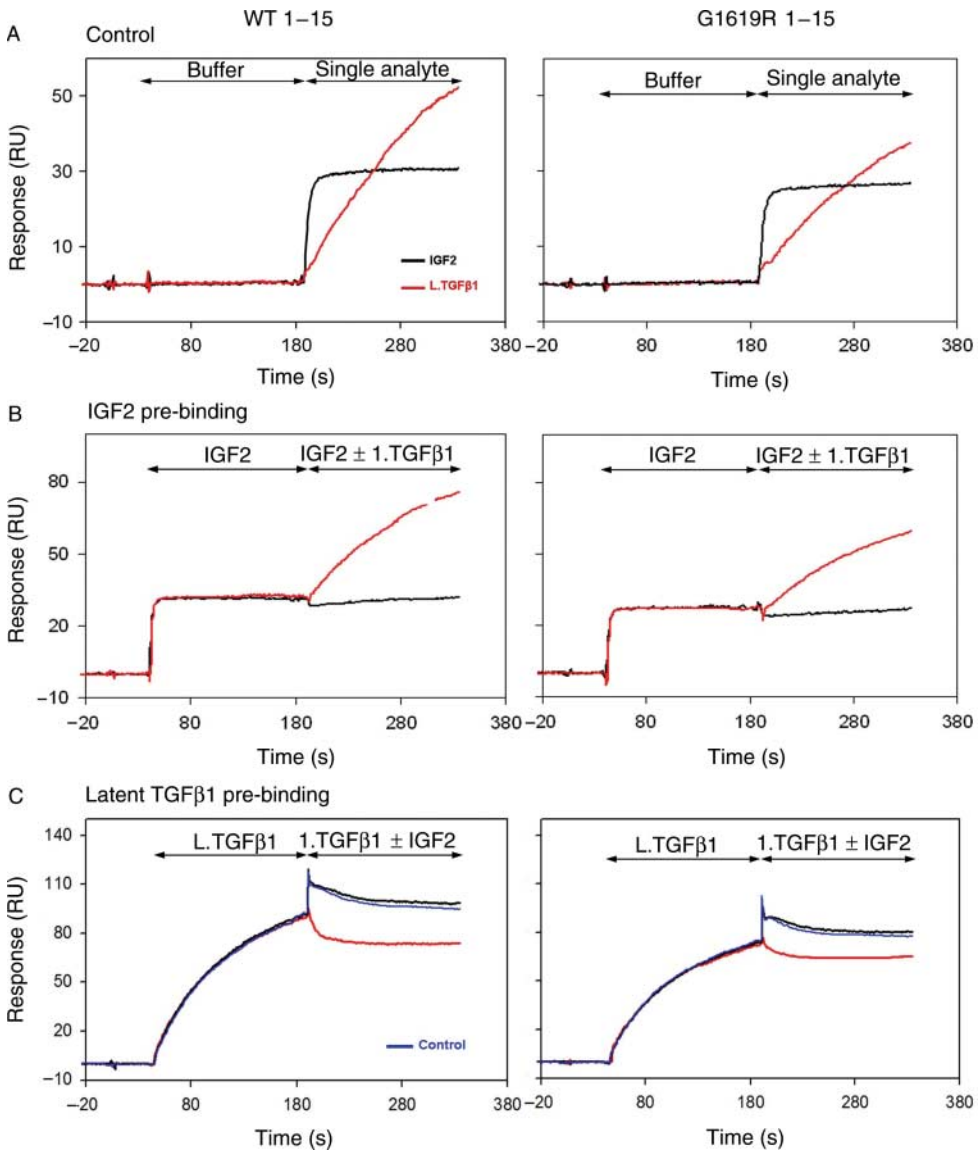

Figure 4 Real-time kinetic evaluation of IGF2 and latent-TGFβ1 competition binding to CD4-chimeric wild-type and G1619R IGF2R domains 1–15. (A) Representative sensorgrams of control 100 μl injections of HBS-EP buffer followed by 100 μl of HBS-EP buffer containing a single analyte, with subsequent binding to immobilised recombinant CD4-chimeric Gly1619 1–15 domains (WT, 1–15) and Arg1619 1–15 domains (G1619R 1–15). 130 nM IGF2 in buffer (black lines), 30 nM latent-TGFβ1 in buffer (red lines) are shown together. (B) The effect of IGF2 pre-binding on the subsequent latent-TGFβ1 binding to WT 1–15 and Gly1619Arg 1–15. Representative sensorgrams are shown. Initial injections of IGF2 (130 nM) alone were followed either by injection of the same concentration of IGF2 (130 nM) in buffer (black lines) or 130 nM IGF2 with 30 nM latent-TGFβ1 (red lines). Similar latent-TGFβ1 binding profiles were observed. (C) The effect of latent-TGFβ1 pre-binding on the subsequent IGF2 binding to WT 1–15 and Gly1619 Arg 1–15. Injections of latent-TGFβ1 (30 nM) were either followed by injection of 30 nM latent-TGFβ1 in buffer (red lines), 30 nM latent-TGFβ1 plus 130 nM IGF2 (black lines) or 130 nM IGF2 only as control (blue lines). The expected binding profile of IGF2 was not detected, and the extent of inhibition was similar in Gly1619 and Arg1619.

described, we mutated Gly1619 to Arg using site directed mutagenesis, and expressed both soluble His-tagged IGF2R domain 11 using *Pichia pastoris*, and chimeric soluble rat CD4 tagged IGF2R domains 11, 10–13 and 1–15 using 293T cells (Linnell *et al.* 2001, Zaccheo *et al.* 2006). Proteins were expressed and single bands identified on western blots (Fig. 2A). Proteins were biotinylated and immoblised on BIAcore biosensor chips and recombinant IGF2 ligand was passed over the sensor surface at increasing concentration and at high flow-rates (40 μl/min). The resulting sensograms were fitted using a two-state conformational

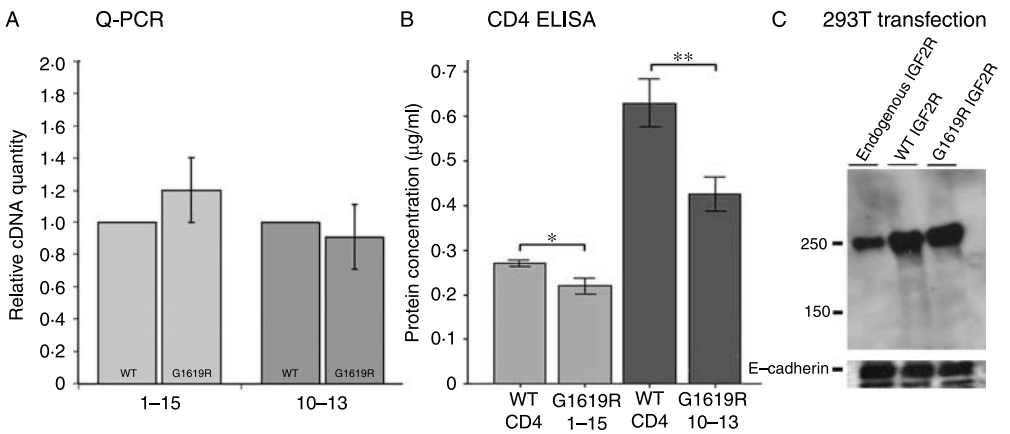

Figure 5 Quantification of mRNA and protein levels in 293T cells transfected with wild-type (WT) and Gly1619Arg IGF2R CD4-1–15. (A) Relative expression of CD4-IGF2R Gly1619Arg mRNA relative to wild-type (1–15 and 10–13) using quantitative RT-PCR. Three separate single comparisons with single value WT taken arbitrarily as 1 and G1619R taken as a ratio. Values are mean ± S.E.M. of three different experiments. Expression was normalised relative to GAPDH. The efficiency of the conducted PCR experiments, as assessed from standard curves, was between 95 and 100%. (B) Quantification of expressed soluble proteins using a CD4 inhibition ELISA suggested that there was no difference in CD4-1–15 proteins but potentially reduced relative amounts of CD4-10–13 Arg1619. Mean ± S.E.M. of six different experiments. *P* values * 0·043, ** 0·015 using students *t*-test. (C) Western blot of endogenous and over-expressed wild-type and G1619R membrane bound IGF2R 1–15 (non-CD4 chimeric) in transfected 293T cell lysates. Samples were subjected to SDS-PAGE and probed with rabbit anti-human IGF2R. The blot was re-probed using rabbit anti-E-cadherin loading control.

change model with BIA evalution software (examples shown in Fig. 2B–D). We had previously validated these biosensor kinetic assays and have shown them to be sensitive enough to detect subtle changes in binding kinetics with single point mutations (Zaccheo *et al.* 2006). Comparison of domain 11 alone, domains 10–13 and domains 1–15 with and without Gly1619Arg showed no significant difference in association and dissociation kinetics (Table 1). Moreover, when biotinylated IGF2 was immobilised, the binding profiles of soluble receptor constructs showed mass transport effects but no differences between Gly1619 and Arg1619, suggesting that differences were not masked by any tethering effect of immobilised receptors (not shown). Thus, we could not detect any difference in affinity between Gly1619 and Arg1619 using single and multiple domain recombinant proteins and SPR.

Real-time analysis of mannose 6-phosphate ligand binding using SPR

We next tested the effects of the Gly1619Arg mutant domain 1–15 proteins on binding to mannose 6-phosphate. For this reaction, we utilised mannosylated latent-TGFβ1 that we had previously tested (Linnell *et al.* 2001, Zaccheo *et al.* 2006). Concentration dependent binding sensorgrams were fitted using a global model (expected stoichiometry of 2:1, Fig. 3 representative sensorgrams) and association and dissociation rates calculated (Table 1). Again, we could not detect significant differences in binding to latent-TGFβ1 alone. Previous reports suggested that binding of IGF2 and latent-TGFβ1 to IGF2R may be mutually exclusive (Kiess *et al* 1989, 1990). In order to test the hypothesis that Gly1619Arg mutation might have altered these interactions, we designed an experiment where either IGF2 or latent-TGFβ1 was pre-bound to immobilised biotinylated CD4-1–15 on a streptavidin biosensor chip (Fig. 4). Kinetics of binding to single analyte was first compared (Fig. 4A), before IGF2 was pre-bound at 130 nM (saturation concentration), followed by latent-TGFβ1 (30 nM) combined with IGF2 (130 nM; Fig. 4B). Examination of sensorgrams revealed similar binding of latent-TGFβ1 irrespective of whether IGF2 was pre-bound (Fig. 4B). However, when latent-TGFβ1 was loaded on the sensor chip prior to IGF2, the subsequent binding of IGF2 was significantly impaired when co-injected with latent-TGFβ1 or alone as a control, indicating that occupied mannose 6-phosphate binding sites impaired IGF2 binding. There were no significant differences in binding kinetics detected between Gly1619 (wild-type) and Arg1619 (Fig. 4C). Thus, we confirmed previous reports that mannose 6-phosphate binding may compete with the IGF2 interaction, an effect presumed to be due to steric hindrance, although indirect conformational changes in binding loops of domains 3 and 9 have not been excluded (Kiess *et al.* 1989, 1990).

A CD4-1–15 IGF2R pulse-chase (1 h pulse)

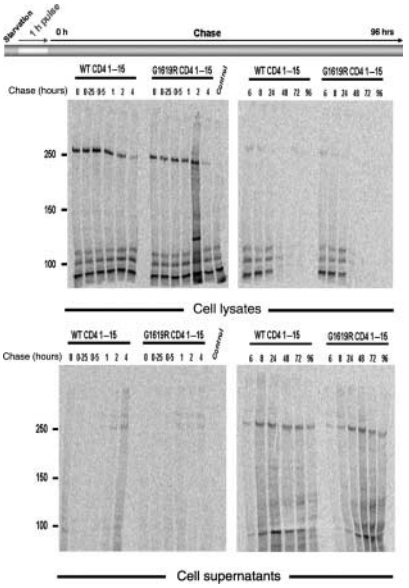

B 1 h pulse (CD4-1–15 IGF2R)

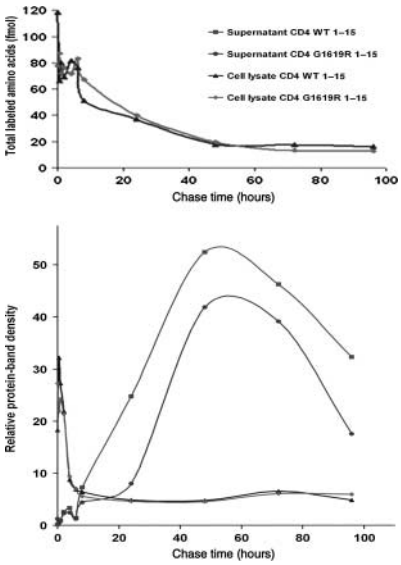

C 1–15 IGF2R pulse-chase (1 h pulse)

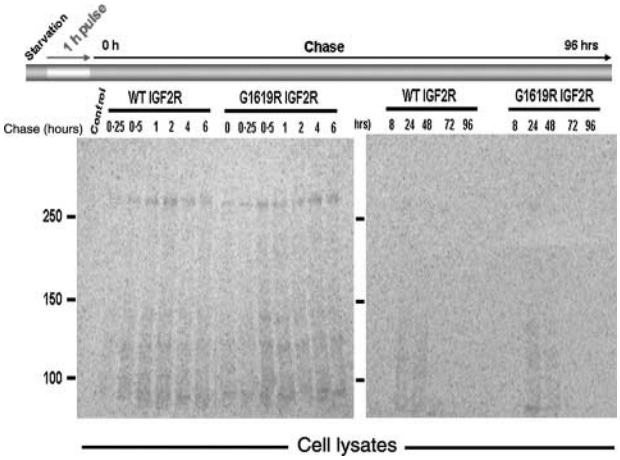

D 1 h pulse (1–15 IGF2R)

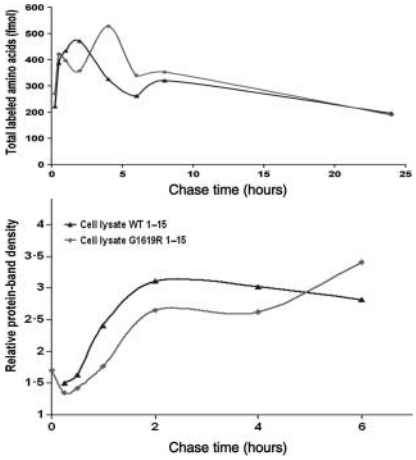

E 1–15 IGF2R pulse-chase (12 h pulse)

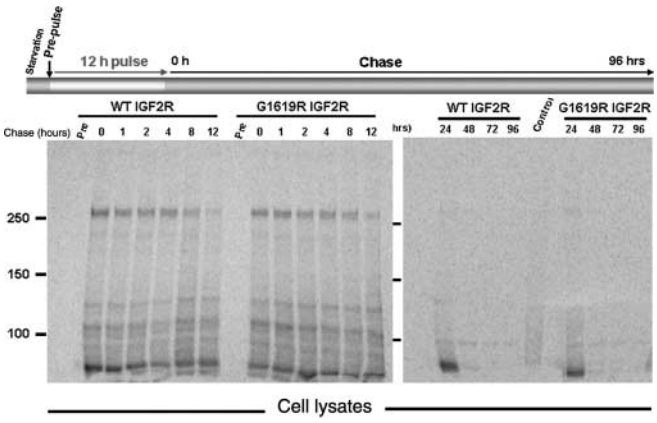

F 12 h pulse (1–15 IGF2R)

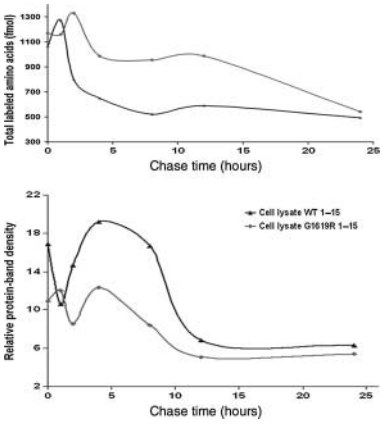

Expression and half-life of IGF2R Gly1619 and Arg1619 in mammalian cells

In order to determine whether the polymorphism altered either RNA or protein stability, we transiently over-expressed both soluble and membrane bound versions of IGF2R domains 1–15 in 293T cells. Messenger RNA expression and protein levels were quantified using quantitative RT-PCR and a previously described CD4 inhibition ELISA (for soluble CD4-1–15 proteins) respectively (Davis *et al.* 1990, Linnell *et al.* 2001). No significant changes in mRNA levels and 1–15 protein constructs were detected (Fig. 5A and C), although a significant relative reduction in level of the CD4-10–13 Arg1619 and CD4-1–15 Arg1619 was observed. It was possible that either selective proteolysis or alteration in protein half-life accounted for these results with CD4 chimeric proteins, the former a mechanism of IGF2R turnover (Clairmont and Czech 1991), the latter having been described for mutations of the membrane receptors (Nakayama *et al.* 2004, Sharma *et al.* 2004).

In order to further investigate these results, we next performed ^{35}S-methionine pulse-chase experiments in 293T cells transiently transfected with CD4-1–15 Gly1619 and CD4-1–15 Arg 1619 to generate soluble proteins, and 1–15Gly1619 and 1–15Arg1619 to generate membrane bound proteins. Cell lysate and supernatant samples were immuno-precipitated with antibodies to either CD4 or IGF2R depending on whether soluble or membrane bound proteins were expressed respectively. SDS protein gels were exposed and quantified by phosphorimaging, and radioactivity expressed relative to a control of the total radioactivity in the sample. Following a 1 h pulse and 96 h chase, soluble CD4-1–15 proteins were chased into the supernatants from cell lysates with similar kinetics and levels between Gly1619 and Arg1619 (Fig. 6A and B). For membrane bound proteins, a 12 h pulse resulted in higher radio-labelled protein levels in cell lysates compared with a 1 h pulse, with no significant overall differences observed between Gly1619 and Arg1619 half-life in cell lysates and cell culture supernatants (Fig. 6C–F). We concluded that differences in protein abundance observed following transient transfection were not related to altered half-life of IGF2R proteins.

Surface membrane distribution of IGF2R protein

Finally, we utilised membrane bound 1–15 Gly1619 and Arg1619 co-expressed with eGFP reporter plasmid following transient co-transfection in order to determine whether membrane distribution of IGF2R was altered. Immuno-fluorescence of unfixed cells with a mouse anti-human IGF2R antibody did not show altered distribution with Arg1619 (not shown). Two colour flow cytometry was then utilised to quantify surface expression of IGF2R in unfixed 293T cells and total IGF2R in cells that had been fixed and permeablised (Fig. 7). Following control transfections to set thresholds of detection (not shown), eGFP positive and PE/Cy5 anti-IGF2R positive cells were quantified, and again showed no differences in abundance and membrane protein localisation between genotypes.

Genetic variation around IGF2R Gly1619Arg

The frequency of the rs624849, Exon 34–93 A>G, Gly1619Arg SNP is variable between different human populations. Using publicly available databases, population-specific genetic variation and linkage disequilibrium (LD) of Gly1619Arg was evaluated. The frequency of the A allele ranged from 0 in the HapMap Yoruba subjects to 0.25 in Pacific Rim subjects from SNP500Cancer (Table 2). This SNP was not in Hardy–Weinberg equilibrium in Caucasian subjects from both HapMap and SNP500Cancer.

LD was assessed between rs629849 and SNPs 20 kb upstream and downstream of rs629849 with minor allele frequencies greater than or equal to 0·01. rs629849 was not in strong LD ($R^2 > 0{\cdot}8$) with any SNPs in these regions. SNPs with R^2 values greater than 0·3 and D′ values >0·8, suggestive, but not strongly

Figure 6 IGF2R [^{35}S] radiolabelled pulse-chase in transfected 293T cells. (A and B) Soluble CD4-IGF2R chimeric proteins. Pulse-chase analysis of IGF2R wild-type and Gly1619Arg CD4-1–15 processing by 293T cells transiently transfected and pulsed for 1 h with [^{35}S]-cysteine and [^{35}S]-methionine, and chased in cold media as described in methods. Supernatants and cell lysates were collected at chase time points as indicated, immuno-precipitated using mouse anti-rat CD4 antibody, and subjected to SDS-PAGE. Controls were either cell lysates or supernatants of non-transfected 293T cells. Densitometry data (B) were obtained from phosphor-imager scanned protein bands (times as indicated) and measured using ImageQuant software and normalised against total [^{35}S] liquid scintillation per chase sample (A). (B) Upper curves depict the total [^{35}S] liquid scintillation counts of 50 μl samples of corresponding cell lysates. (C—F) Membrane bound non-CD4 IGF2R. Pulse-chase analysis of wild-type and Gly1619Arg membrane bound 1–15 IGF2R (non-CD4 chimeric) processing by 293T cells. Transiently transfected 293T cells that expressed wild-type or Gly1619Arg 1–15 IGF2R were pulsed for 1 h (C and D) or 12 h (E and F) with [^{35}S]-cysteine and [^{35}S]-methionine, then chased in cold media. Cell lysates were collected at various chase time points (as indicated) and immuno-precipitated using mouse anti-human IGF2R antibody, and then subjected to SDS-PAGE to detect 1–15 IGF2R. Controls are cell lysates of non-transfected 293T cells and pre-pulse samples (Pre) were taken prior to metabolic labelling. Again, example phosphor-images (C and E) were quantified using ImageQuant software and normalised against total [^{35}S] liquid scintillation per chase sample. (D) and (F) The upper curves depict the total [^{35}S] liquid scintillation counting of 50 μl cell lysates and the lower curves depict the relative band intensity.

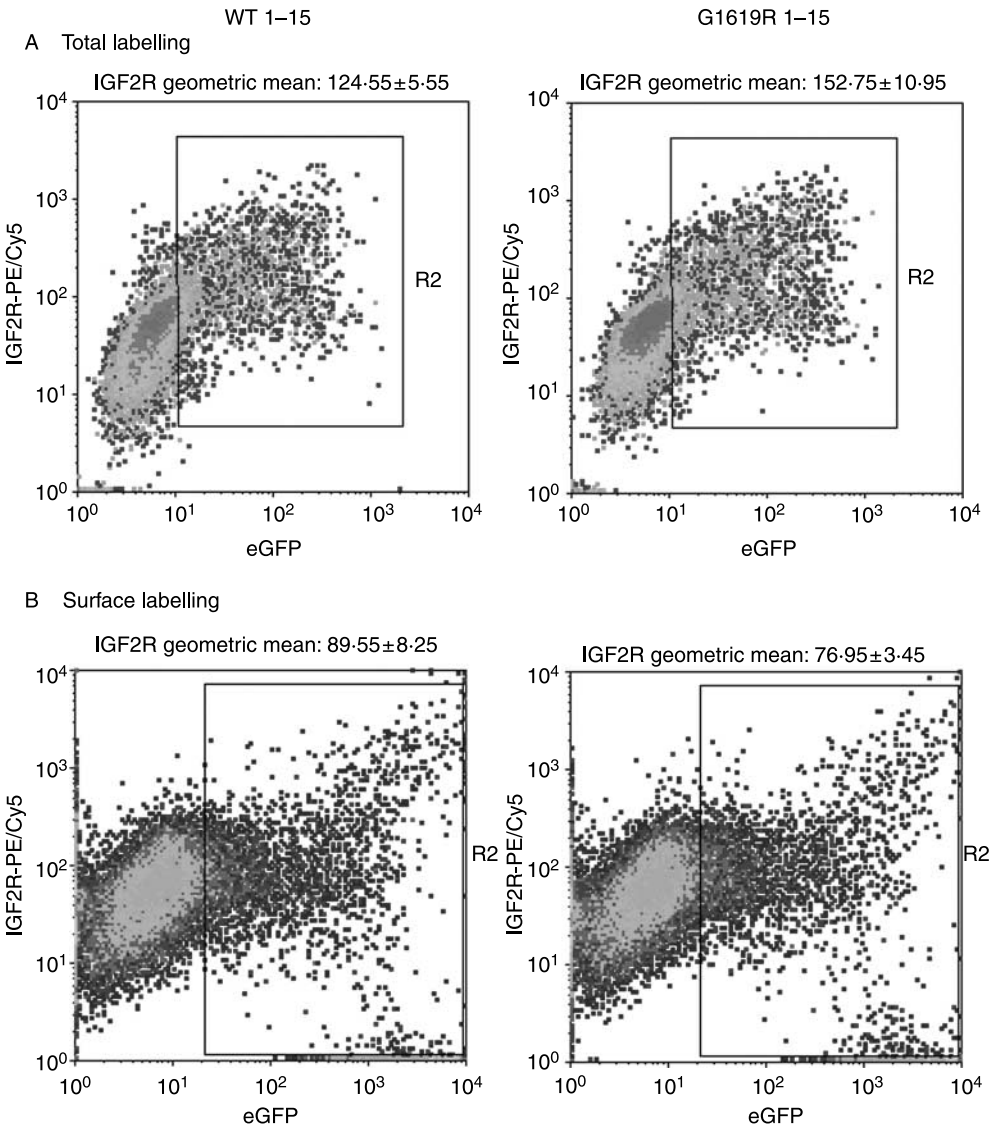

Figure 7 Flow cytometry of anti-IGF2R labelled 293T cells over-expressing membrane bound IGF2R domains 1–15. 293T cells were co-transfected with membrane bound (non-CD4 chimeric) IGF2R 1–15 (pcDNA IGF2R) and eGFP (pEGFP-N1) plasmids as described in methods. Forty-eight h post-transfection, cells were either fixed with paraformaldehyde (2% w/v) or permeablised with Triton X100 (0·1% v/v) (A) or fixed with 4% (w/v) paraformaldehyde alone (B). Cells were incubated with mouse anti-human IGF2R, detected using PE/Cy5 secondary antibody (goat anti-mouse), co-labelling data collected with a FACSCalibur flow cytometer with minimal compensation, and then analysed using WinMDI 2.8 software. Non-transfected and secondary antibody controls were used to set background thresholds (not shown) Geometric means of staining are expressed ±S.E.M. (n=5).

supportive of LD, were noted in subjects of Asian descent from HapMap and SNP500 (Table 3). These SNPs were in nearby introns.

Discussion

Disruption of the function of IGF2R has potent consequences for IGF2 dependent overgrowth of the mammalian embryo (Wang *et al.* 1994, Ludwig *et al.* 1996, Wylie *et al.* 2003). Frequent mutation and loss of function of IGF2R in human tumours have also implicated the selective growth advantage of cells lacking IGF2R (De Souza *et al.* 1995, Hankins *et al.* 1996, Byrd *et al.* 1999, Kong *et al.* 2000). Of the ligands that bind IGF2R, IGF2 appeared to be the most potent in terms of gross effects on growth control. As IGF2 binds IGF2R at a selective binding site in domain 11,

Table 2 Genetic variation of rs629849 (Ex34–93 A>G, Gly1619Arg) amongst populations

	Population	Number of individuals	A allele frequency
HapMap[a]	Han Chinese	42	0·143
	Japanese	43	0·174
	Yoruba	60	0
SNP500Cancer	African/African American	24	0·021
	Caucasian[b]	31	0·194
	Hispanic	23	0·130
	Pacific Rim	24	0·250
Multi-ethnic Cohort	Black	69	0·029
	Hawaiian	69	0·094
	Japanese	68	0·114
	Latino	69	0·066
	White	68	0·103

[a]Data from CEPH Caucasians were not available from HapMap.
[b]rs629849 was not in Hardy–Weinberg equilibrium in this group.

and with high affinity, any non-synonymous polymorphisms of this domain remain strong candidate modifiers of human embryonic and tumour growth.

A number of observational approaches have been taken to assess the functional significance of the 1619 position of domain 11 of IGF2R. During evolution of IGF2R, the receptor acquired an IGF2 ligand binding function that was associated with a number of amino acid mutations of the domain 11 binding site, yet Gly1619 appeared to be a highly conserved amino acid during the evolution of birds (chicken) to mammals (Clairmont and Czech 1989, Yandell *et al.* 1999, Brown *et al.* 2002, 2008). This evolutionary observation suggested that the non-synonymous SNP at 1619 would be unlikely to be involved in a direct interaction with IGF2. Our structural studies have also supported this notion, as the 1619 residue was remotely located with respect to the IGF2 binding site. In addition, IGF2 induced conformational changes in the binding site loop residues but not the 1619 residue, and suggested that any effect on IGF2 binding was likely to be indirect. Modelling of Arg1619 supported potential indirect effects on the FnII domain that subsequently may have lead to alteration of binding site interactions through the AB loop (Zaccheo *et al.* 2006). These observations led us to directly mutate Gly1619 to Arg1619 and to compare receptor function.

A report had correlated slower human childhood growth rate in the rare IGF2R Arg1619 (A/A) homozygotes, yet our data suggested that this amino acid change alone was non-functional in terms of IGF2 and mannose 6-phosphate ligand binding, protein half-life and cell membrane distribution (Petry *et al.* 2005). It is important to state that the implications of our experiments do not alter the interpretation of the

Table 3 Single nucleotide polymorphisms in linkage disequilibrium with rs629849 (Ex34–93 A>G, Gly1619Arg)

Population (number of SNPs in region)	SNP	SNP location	D′	Nighty-five per-cent CI	LOD score	R^2	Distance from rs629849 (bp)
HapMap Han Chinese (31)	rs2282141	IVS39+400	0·875	0·55–0·97	4·35	0·359	7298
	rs3798178	IVS41+1315	0·873	0·54–0·97	4·23	0·356	13 069
	rs3798176	IVS41−893	0·875	0·55–0·97	4·35	0·359	13 763
	rs1888727	IVS44−2930	0·875	0·55–0·97	4·35	0·359	20 132
HapMap Japanese (30)	rs2282141	Ivs39+400	1	0·75–1	6·88	0·488	7298
	rs2343275	Ivs39+1420	1	0·75–1	7·16	0·538	8318
	rs3798178	Ivs41+1315	1	0·73–1	6·42	0·469	13 069
	rs3798176	Ivs41−893	1	0·75–1	6·88	0·488	13 763
	rs1888727	Ivs44−2930	0·895	0·61–0·97	5·26	0·413	20 132
SNP500Cancer Pacific Rim (5)	rs3798180	Ivs31+651	1	0·7–1	6·29	0·509	2668

SNPs with minor allele frequencies ≥ 0·01 20 kb upstream and downstream of rs629849 were evaluated for linkage disequilibrium in the populations shown. SNPs with R^2 values > 0·3 are reported. Abbreviations: SNP, single nucleotide polymorphism; CI, confidence interval for D′; LOD score, log of the likelihood ratio, a measure of the confidence in the value of D′; R^2, the correlation coefficient between the two loci.

positive correlation between circulating concentrations of IGF2, and inverse correlation with soluble IGF2R and human growth (Ong *et al.* 2000, Garrone *et al.* 2002). However, our data make it difficult to directly attribute the phenotypic growth effects with Gy1619Arg to IGF2R receptor function. Even though the observations of Petry *et al.* (2005) are unconfirmed, our observations do not alter the Arg1619 correlation observed (Kaku *et al.* 2007), as there are a number of potential explanations that might reconcile these sets of data.

Firstly, it was possible the assays we utilised may have been insensitive to subtle changes in receptor function. For real-time analysis of recombinant protein interactions, we are confident that the validated approach taken here would have been sensitive enough to define functional variation, such as the fundamental binding interaction between IGF2 and IGF2R. This was unaltered between Gly1619 and Arg1619. Importantly, we have also shown that the competitive binding between mannose 6-phosphate and IGF2 binding was also unaltered. As IGF2R cycles between the endoplasmic reticulum, Golgi and the pre-lysosomal compartment, it was possible that modified function may have occurred as a result of either altered trafficking, distribution or proteolysis (Ghosh *et al.* 2003). It is well established that the trafficking and distribution functions of IGF2R depend on the cytoplasmic domain that is remotely located with respect to 1619, which meant that it would have been highly unlikely that Gly1619Arg would have altered trafficking. However, several important non-synonymous polymorphisms of membrane receptors have functional effects that were related to altered protein half-life. For example, the chemokine receptor *CCR2-Val64Ile* polymorphism resulted in protein with prolonged half-life that had explained the delayed progression to AIDS in HIV infected humans with 64Ile (Nakayama *et al.* 2004). In addition, deletion of Phe508 of the *CFTR* gene leads to cystic fibrosis because of altered folding, stability and plasma membrane half-life (Sharma *et al.* 2004). Here, we directly addressed this question and performed quantitative pulse-chase and flow cytometry experiments that suggested that Gly1619Arg did not significantly alter the rate of protein production, processing, proteolysis and membrane distribution. The only remaining functional mechanism that we did not directly test was the potential interaction of residue 1619 with domain 12, and the potential for indirect modification of IGF2R dimerisation (Kreiling *et al.* 2005). We have previously detected dimerisation of 1–4% of recombinant domain 11–12 and 11–13 using analytical ultracentrifugation, corroborating our observation of structural juxtaposition of domain 12 in crystals and the data obtained using epitope tagged IGF2R (Kreiling *et al.* 2005, Brown *et al.* 2008). Ligand binding does not alter the ability of IGF2R to dimerise, but dimerisation may improve the avidity of the receptor for ligands and increase the rate of internalisation (York *et al.* 1999, Byrd *et al.* 2000). Detailed examination of our crystal structures confirmed that Gly1619R was remote from the hydrophobic dimerisation surface in domain 12 that involved Pro1755 and Tyr1741, and that there appeared no conformational change in position of 1619 when comparing crystals from domains 11–12 (where there is no dimerisation) with those of 11–13 (where there is dimersiation) (not shown, Brown *et al.* (2008)). These observations suggested that Gly1619Arg would be unlikely to alter the extent and stability of IGF2R dimerisation, particularly as multiple domain interactions that regulate dimerisation avidity between full length receptors.

Our data leads us to conclude that the Gly1619Arg polymorphism is non-functional. It is possible that there could be interactions with other non-synonymous SNPs. For example, the location of the Gln1696Arg (rs11552587) residue appeared closely localised to Gly1619Arg in the crystal structure (Fig. 8), and may directly interact to modify function. However, this SNP is very rare in the populations examined so far (e.g. 0·009 allelic frequency in the Yoruba) and means that it was unlikely that this interaction would be significant. However, it is possible that in certain populations the rs629849 SNP is in LD with others that could contribute to differential function or expression of the IGF2R gene. Importantly, the SNPs with suggested LD with the

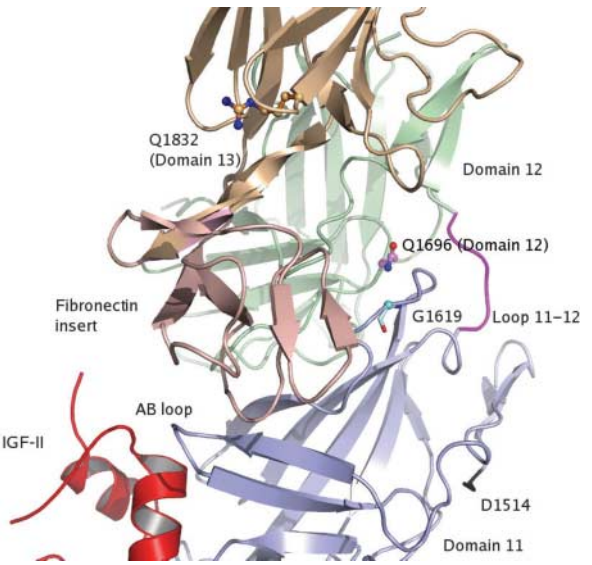

Figure 8 Structural localisation of Gln1696Arg and Gly1619Arg. The rare SNP (rs11552587) results in a non-synonymous polymorphism Gln1696Arg that modifies an amino acid that also locates close to Gly1619Arg in the region between domains 11, 12 and 13. Other potential non-synonymous amino acids are also shown (Gln/Q1832, Asp/D1514), but none are in linkage disequilibrium with rs629849.

Gly1619Arg polymorphism were in intronic sequences and could possibly affect intron–exon splice sites. Functional associations need not be correlated with exon SNPs, as functional consequences may occur as a result of intron SNPs, for example recently implicated in altered methylation (Savage *et al.* 2007). Alternatively, other non-synonymous SNPs in other regions of the protein may result in unpredictable functional changes. In order to completely understand the complex function of the IGF2R protein and the effect of genetic polymorphisms on its function, further experimental evaluation of IGF2R polymorphisms are warranted.

Declaration of interest

The authors declare that there is no conflict of interest that could be perceived as prejudicing the impartiality of the research reported.

Funding

Supported by Cancer Research UK (C429, C375), Wellcome Trust and NIH. This research was supported (in part) by the Intramural Research Program of the National Institutes of Health, National Cancer Institute, Division of Cancer Epidemiology and Genetics.

Acknowledgements

We thank James Brown, Emily Foulstone, David Barnes and John Crosby for discussion, Cancer Research UK (ABH- C429, EYJ-C375), Wellcome Trust UK (MC-082352) and an Algerian Ministry of Higher Education Scholarship (DR) for funding.

References

Barrett JC, Fry B, Maller J & Daly MJ 2005 Haploview: analysis and visualization of LD and haplotype maps. *Bioinformatics* **21** 263–265.

Brown J, Esnouf RM, Jones MA, Linnell J, Harlos K, Hassan AB & Jones EY 2002 Structure of a functional IGF2R fragment determined from the anomalous scattering of sulfur. *EMBO Journal* **21** 1054–1062.

Brown J, Delaine C, Zaccheo OJ, Siebold C, Gilbert RJ, van Boxel G, Denley A, Wallace JC, Hassan AB, Forbes BE *et al.* 2008 Structure and functional analysis of the IGF-II/IGF2R interaction. *EMBO Journal* **27** 265–276.

Byrd JC, Devi GR, de Souza AT, Jirtle RL & MacDonald RG 1999 Disruption of ligand binding to the insulin-like growth factor II/mannose 6-phosphate receptor by cancer-associated missense mutations. *Journal of Biological Chemistry* **274** 24408–24416.

Byrd JC, Park JH, Schaffer BS, Garmroudi F & MacDonald RG 2000 Dimerization of the insulin-like growth factor II/mannose 6-phosphate receptor. *Journal of Biological Chemistry* **275** 18647–18656.

Christofori G, Naik P & Hanahan D 1994 A second signal supplied by insulin-like growth factor II in oncogene-induced tumorigenesis. *Nature* **369** 414–418.

Clairmont KB & Czech MP 1989 Chicken and Xenopus mannose 6-phosphate receptors fail to bind insulin-like growth factor II. *Journal of Biological Chemistry* **264** 16390–16392.

Clairmont KB & Czech MP 1991 Extracellular release as the major degradative pathway of the insulin-like growth factor II/mannose 6-phosphate receptor. *Journal of Biological Chemistry* **266** 12131–12134.

Conover CA, Bale LK, Overgaard MT, Johnstone EW, Laursen UH, Fuchtbauer EM, Oxvig C & van Deursen J 2004 Metalloproteinase pregnancy-associated plasma protein A is a critical growth regulatory factor during fetal development. *Development* **131** 1187–1194.

Cui H, Cruz-Correa M, Giardiello FM, Hutcheon DF, Kafonek DR, Brandenburg S, Wu Y, He X, Powe NR & Feinberg AP 2003 Loss of IGF2 imprinting: a potential marker of colorectal cancer risk. *Science* **299** 1753–1755.

Davis SJ, Ward HA, Puklavec MJ, Willis AC, Williams AF & Barclay AN 1990 High level expression in Chinese hamster ovary cells of soluble forms of CD4 T lymphocyte glycoprotein including glycosylation variants. *Journal of Biological Chemistry* **265** 10410–10418.

De Souza AT, Hankins GR, Washington MK, Orton TC & Jirtle RL 1995 M6P/IGF2R gene is mutated in human hepatocellular carcinomas with loss of heterozygosity. *Nature Genetics* **11** 447–449 issn: 1061-4036.

Delaglio F, Grzesiek S, Vuister GW, Zhu G, Pfeifer J & Bax A 1995 NMRPipe: a multidimensional spectral processing system based on UNIX pipes. *Journal of Biomolecular NMR* **6** 277–293.

Dennis PA & Rifkin DB 1991 Cellular activation of latent transforming growth factor beta requires binding to the cation-independent mannose 6-phosphate/insulin-like growth factor type II receptor. *PNAS* **88** 580–584.

Devi GR, De Souza AT, Byrd JC, Jirtle RL & MacDonald RG 1999 Altered ligand binding by insulin-like growth factor II/mannose 6-phosphate receptors bearing missense mutations in human cancers. *Cancer Research* **59** 4314–4319.

Foulstone E, Prince S, Zaccheo O, Burns JL, Harper J, Jacobs C, Church D & Hassan AB 2005 Insulin-like growth factor ligands, receptors, and binding proteins in cancer. *Journal of Pathology* **205** 145–153.

Frazer KA, Ballinger DG, Cox DR, Hinds DA, Stuve LL, Gibbs RA, Belmont JW, Boudreau A, Hardenbol P, Leal SM *et al.* 2007 A second generation human haplotype map of over 3·1 million SNPs. *Nature* **449** 851–861.

Garrone S, Radetti G, Sidoti M, Bozzola M, Minuto F & Barreca A 2002 Increased insulin-like growth factor (IGF)-II and IGF/IGF-binding protein ratio in prepubertal constitutionally tall children. *Journal of Clinical Endocrinology and Metabolism* **87** 5455–5460.

Ghosh P, Dahms NM & Kornfeld S 2003 Mannose 6-phosphate receptors: new twists in the tale. *Nature Reviews. Molecular Cell Biology* **4** 202–212.

Hancock MK, Haskins DJ, Sun G & Dahms NM 2002*a* Identification of residues essential for carbohydrate recognition by the insulin-like growth factor II/mannose 6-phosphate receptor. *Journal of Biological Chemistry* **277** 11255–11264.

Hancock MK, Yammani RD & Dahms NM 2002*b* Localization of the carbohydrate recognition sites of the insulin-like growth factor II/mannose 6-phosphate receptor to domains 3 and 9 of the extracytoplasmic region. *Journal of Biological Chemistry* **277** 47205–47212.

Hankins GR, De Souza AT, Bentley RC, Patel MR, Marks JR, Iglehart JD & Jirtle RL 1996 M6P/IGF2, receptor: a candidate breast tumor suppressor gene. *Oncogene* **12** 2003–2009.

Harper J, Burns JL, Foulstone EJ, Pignatelli M, Zaina S & Hassan AB 2006 Soluble IGF2 receptor rescues Apc(Min/+) intestinal adenoma progression induced by Igf2 loss of imprinting. *Cancer Research* **66** 1940–1948.

Ito Y, Koessler T, Ibrahim AE, Rai S, Vowler SL, Abu-Amero S, Silva AL, Maia AT, Huddleston JE, Uribe-Lewis S *et al.* 2008 Somatically acquired hypomethylation of IGF2 in breast and colorectal cancer. *Human Molecular Genetics* **17** 2633–2643.

Kaku K, Osada H, Seki K & Sekiya S 2007 Insulin-like growth factor 2 (IGF2) and IGF2 receptor gene variants are associated with fetal growth. *Acta Paediatrica* **96** 363–367.

Kalscheuer VM, Mariman EC, Schepens MT, Rehder H & Ropers HH 1993 The insulin-like growth factor type-2 receptor gene is imprinted in the mouse but not in humans. *Nature Genetics* **5** 74–78.

Kiess W, Thomas CL, Greenstein LA, Lee L, Sklar MM, Rechler MM, Sahagian GG & Nissley SP 1989 Insulin-like growth factor-II (IGF-II) inhibits both the cellular uptake of beta-galactosidase and the binding of beta-galactosidase to purified IGF-II/mannose 6-phosphate receptor. *Journal of Biological Chemistry* **264** 4710–4714.

Kiess W, Thomas CL, Sklar MM & Nissley SP 1990 Beta-galactosidase decreases the binding affinity of the insulin-like-growth-factor-II/mannose-6-phosphate receptor for insulin-like-growth-factor II. *European Journal of Biochemistry* **190** 71–77.

Killian JK, Oka Y, Jang HS, Fu X, Waterland RA, Sohda T, Sakaguchi S & Jirtle RL 2001 Mannose 6-phosphate/insulin-like growth factor 2 receptor (M6P/IGF2R) variants in American and Japanese populations. *Human Mutation* **18** 25–31.

Kolonel LN, Altshuler D & Henderson BE 2004 The multiethnic cohort study: exploring genes, lifestyle and cancer risk. *Nature Reviews. Cancer* **4** 519–527.

Kong FM, Anscher MS, Washington MK, Killian JK & Jirtle RL 2000 RLM6P/IGF2R, is mutated in squamous cell carcinoma of the lung. *Oncogene* **19** 1572–1578.

Kreiling JL, Byrd JC & MacDonald RG 2005 Domain interactions of the mannose 6-phosphate/insulin-like growth factor II receptor. *Journal of Biological Chemistry* **280** 21067–21077.

Linnell J, Groeger G & Hassan AB 2001 Real time kinetics of insulin-like growth factor II (IGF-II) interaction with the IGF-II/mannose 6-phosphate receptor: the effects of domain 13 and pH. *Journal of Biological Chemistry* **276** 23986–23991.

Ludwig T, Eggenschwiler J, Fisher P, D'Ercole AJ, Davenport ML & Efstratiadis A 1996 Mouse mutants lacking the type 2 IGF receptor (IGF2R) are rescued from perinatal lethality in Igf2 and Igf1r null backgrounds. *Developmental Biology* **177** 517–535 issn: 0012-1606.

Nakayama EE, Tanaka Y, Nagai Y, Iwamoto A & Shioda T 2004 A CCR2-V64I polymorphism affects stability of CCR2A isoform. *AIDS* **18** 729–738.

Ong K, Kratzsch J, Kiess W, Costello M, Scott C & Dunger D 2000 Size at birth and cord blood levels of insulin, insulin-like growth factor I (IGF-I), IGF-II, IGF-binding protein-1 (IGFBP-1), IGFBP-3, and the soluble IGF-II/mannose-6-phosphate receptor in term human infants, The ALSPAC study team. Avon longitudinal study of pregnancy and childhood. *Journal of Clinical Endocrinology and Metabolism* **85** 4266–4269.

Packer BR, Yeager M, Burdett L, Welch R, Beerman M, Qi L, Sicotte H, Staats B, Acharya M, Crenshaw A *et al.* 2006 SNP500Cancer: a public resource for sequence validation, assay development, and frequency analysis for genetic variation in candidate genes. *Nucleic Acids Research* **34** D617–D621.

Petry CJ, Ong KK, Wingate DL, Brown J, Scott CD, Jones EY, Pembrey ME & Dunger DB 2005 Genetic variation in the type 2 insulin-like growth factor receptor gene and disparity in childhood height. *Growth Hormone and IGF Research* **15** 363–368.

Savage SA, Woodson K, Walk E, Modi W, Liao J, Douglass C, Hoover RN & Chanock SJ 2007 Analysis of genes critical for growth regulation identifies Insulin-like Growth Factor 2 Receptor variations with possible functional significance as risk factors for osteosarcoma. *Cancer Epidemiology Biomarkers & Prevention* **16** 1667–1674.

Sharma M, Pampinella F, Nemes C, Benharouga M, So J, Du K, Bache KG, Papsin B, Zerangue N, Stenmark H *et al.* 2004 Misfolding diverts CFTR from recycling to degradation: quality control at early endosomes. *Journal of Cell Biology* **164** 923–933.

Vranken WF, Boucher W, Stevens TJ, Fogh RH, Pajon A, Llinas M, Ulrich EL, Markley JL, Ionides J & Laue ED 2005 The CCPN, data model for NMR spectroscopy: development of a software pipeline. *Proteins* **59** 687–696.

Wang ZQ, Fung MR, Barlow DP & Wagner EF 1994 Regulation of embryonic growth and lysosomal targeting by the imprinted Igf2/Mpr gene. *Nature* **372** 464–467.

Williams C, Rezgui D, Prince SN, Zaccheo OJ, Foulstone EJ, Forbes BE, Norton RS, Crosby J, Hassan AB & Crump MP 2007 Structural insights into the interaction of insulin-like growth factor 2 with IGF2R domain 11. *Structure* **15** 1065–1078.

Wutz A, Theussl HC, Dausman J, Jaenisch R, Barlow DP & Wagner EF 2001 Non-imprinted Igf2r expression decreases growth and rescues the Tme mutation in mice. *Development* **128** 1881–1887.

Wylie AA, Pulford DJ, McVie-Wylie AJ, Waterland RA, Evans HK, Chen YT, Nolan CM, Orton TC & Jirtle RL 2003 Tissue-specific inactivation of murine M6P/IGF2R. *American Journal of Pathology* **162** 321–328.

Xu Y, Goodyer CG, Deal C & Polychronakos C 1993 Functional polymorphism in the parental imprinting of the human IGF2R gene. *Biochemical and Biophysical Research Communication* **197** 747–754.

Yandell CA, Dunbar AJ, Wheldrake JF & Upton Z 1999 The kangaroo cation-independent mannose 6-phosphate receptor binds insulin-like growth factor II with low affinity. *Journal of Biological Chemistry* **274** 27076–27082.

York SJ, Arneson LS, Gregory WT, Dahms NM & Kornfeld S 1999 The rate of internalization of the mannose 6-phosphate/insulin-like growth factor II receptor is enhanced by multivalent ligand binding. *Journal of Biological Chemistry* **274** 1164–1171.

Young LE, Fernandes K, McEvoy TG, Butterwith SC, Gutierrez CG, Carolan C, Broadbent PJ, Robinson JJ, Wilmut I & Sinclair KD 2001 Epigenetic change in IGF2R is associated with fetal overgrowth after sheep embryo culture. *Nature Genetics* **27** 153–154.

Zaccheo OJ, Prince SN, Miller DM, Williams C, Kemp CF, Brown J, Jones EY, Catto LE, Crump MP & Hassan AB 2006 Kinetics of insulin-like growth factor II (IGF-II) interaction with domain 11 of the human IGF-II/mannose 6-phosphate receptor: function of CD and AB loop solvent-exposed residues. *Journal of Molecular Biology* **359** 403–421.

Received in final form 8 January 2009
Accepted 4 February 2009
Made available online as an Accepted Preprint 4 February 2009